1

PARTICLE MOTION IN A SINGLE VORTEX

•

Burgers vortex [**Burgers_1948**] is used as a model of a steady vortex tube. The z-axis in the cylindrical coordinate system (r, φ, z) is aligned with the vortex axis. 3D velocity field $\vec{v}$ is determined by two parameters: circulation Γ and stretching strength γ:

$$\vec{v} = -\frac{\gamma}{2} r \hat{e}_r + \frac{\Gamma}{2\pi r}\left(1 - e^{-\frac{r^2}{2\delta^2}}\right)\hat{e}_\varphi + \gamma z \hat{e}_z, \tag{1}$$

where $\delta = \sqrt{2\nu/\gamma}$ is the vortex core size and ν denotes the kinematic viscosity.
Definition of azimuthal velocity introduces a spatial scale into the system: r_s. Azimuthal velocity reaches its maximum at $r = r_s\delta$. Analytically $r_s = \sqrt{(}-2W(1, -exp(-1/2)/2) - 1)$, where $W(k, x)$ denotes Lambert W functions' kth branch of x. What is more useful for the purposes of this thesis is the numerical estimation: $r_s \approx 1.5852011$.
A particle's equation of motion includes the terms ... . of Eq.**??** and is as follows:

$$\ddot{\vec{r}} = \frac{1}{\tau_p}\left(\vec{v} - \dot{\vec{r}}\right) + \vec{g}, \tag{2}$$

where τ_p is the particle relaxation time and $\vec{g} = -g\left(\sin\theta \hat{e_y} + \cos\theta \hat{e_z}\right)$ is gravitational acceleration inclined by the angle $\theta \in [0, 90^o]$ with respect to the vortex axis.
The analysis of single droplet motion in projection on a plane (r, φ) perpendicular to the vortex axis (henceforth called 2D space) was conducted by **Marcu_95** and is summarized below. The behavior of a droplet inside the vortex depends on a set of six parameters $\{\Gamma, \gamma, \theta, \tau_p, g, \nu\}$:

$$\begin{cases} \ddot{r} - r\dot{\varphi}^2 = \tau_p^{-1}\left(-\gamma r/2 - \dot{r}\right) - g\sin\theta\sin\varphi \\ 2\dot{r}\dot{\varphi} + r\ddot{\varphi} = \tau_p^{-1}\left(\frac{\Gamma}{2\pi r}\left(1 - \exp(-\gamma r^2/4\nu)\right) - r\dot{\varphi}\right) - g\sin\theta\cos\varphi \\ \ddot{z} = \tau_p^{-1}\left(\gamma z - \dot{z}\right) - g\cos\theta \end{cases} . \tag{3}$$

The non-dimensionalization of the equations leads to Eq. 4 and gives a set of dimensionless parameters $\{St, S_\nu, \theta, A\}$:

$$\begin{cases} \ddot{r^*} - r^*\dot{\varphi^*}^2 = -St^{-1}\left(Ar^* + \dot{r^*} + S_\nu\sin\varphi\right) \\ 2\dot{r^*}\dot{\varphi^*} + r^*\ddot{\varphi^*} = St^{-1}\left(\frac{1}{2\pi r^*}(1 - e^{-\frac{r^{*2}}{2}}) - r^*\dot{\varphi^*} - S_\nu\cos\varphi\right) \\ \ddot{z^*} = St^{-1}\left(Az - \dot{z^*} - S_\nu\cot\theta\right) \end{cases} . \tag{4}$$

Henceforth, dimensionless variables are denoted by *. Stokes number St here is calculated with the use of the characteristic timescale of the Burgers vortex flow, which is the vortex core rotation time $\tau_f = \delta^2\Gamma^{-1}$, so $St = \tau_p\Gamma\delta^{-2}$. The sedimentation parameter: $S_v = \delta g\tau_p \sin\theta\Gamma^{-1}$. It characterizes motion in a plane perpendicular to the vortex axis. The last quantity $A = \nu\Gamma^{-1} = 1/Re_\nu$ is the non-dimensional strain parameter, the inverse of vortex Reynolds number Re_ν. It is worth mentioning that the ratio of Stokes number to the sedimentation parameter, called Froude number $Fr = StS_\nu^{-1}$, is considered a measure of the influence of gravitational force on the droplet motion. In the limit of a large Froude number, gravity is seen as negligible.
As one can see in Eq.4, the equation describing particle motion along the vortex axis is independent from the equations describing motion in 2D space. Thus there are analyzed seperately below. In this analysis, particular emphasis is placed on describing the characteristic time scales of the motion. The aim was to find a measure to determine whether the motion of a particle differs significantly from the flying through a vortex, in the context of the influence on the spatial distribution of particles.

Motion along the vortex axis

Motion along the vortex axis is determined by stretching outflow drag and gravity force only. As a consequence, the particle z position shows an exponential dependence on time. Small parts of the analytical solution presented below was discussed in [**Kar_2014**].
Solution of the equation of motion's third component with arbitrary constants C_1 and C_2 is:

$$z^*(t) = C_1 \exp\lambda_1 t^* + C_2 \exp\lambda_2 t^* + z_b^* \tag{5}$$

With the initial conditions $z^*(0) = z_0^*$, $\dot{z}(0) = w_0$ the solution is as follows:

$$\frac{z^*(t^*) - z_b^*}{z_0^* - z_b^*} = \frac{1}{\lambda_1 - \lambda_2}\left[\lambda_1 \exp\lambda_2 t^* - \lambda_2 \exp\lambda_1 t^* + \frac{w_0^*}{z_0^* - z_b^*}\left(\exp\lambda_1 t^* - \exp\lambda_2 t^*\right)\right] \tag{6}$$

where $\lambda_{1/2} = \left(\mp\sqrt{1 + 4ASt} - 1\right)/2St$.
The particle with $w_0 = 0$ placed in z_b where:

$$z_b^* = S_\nu A^{-1}\cot\theta = \nu^{-1} g\delta\tau_p cos\theta \sim R^2 \tag{7}$$

is in unstable equilibrium.

Eq.6 is of the dimensional form:

$$\frac{z(t) - z_b}{z_0 - z_b} = \left[\frac{1}{2}(1-k) - k\frac{\tau_p w_0}{z_0 - z_b}\right] e^{\frac{-t}{\tau_z}} + \left[\frac{1}{2}(1+k) + k\frac{\tau_p w_0}{z_0 - z_b}\right] e^{\frac{t}{\tau_z}} \tag{8}$$

where we denote non-dimensional parameter $k = (1 + ASt)^{-1/2} = (1 + \frac{\nu\tau_p}{\delta^2})^{-1/2}$, $k \in (0, 1)$ for conviniency. Dimensional equillibrium position : $z_b = z_b^*\delta = \nu^{-1} g\delta^2\tau_p cos\theta > 0$. Its values for cloud-like conditions are presented in Fig.1.

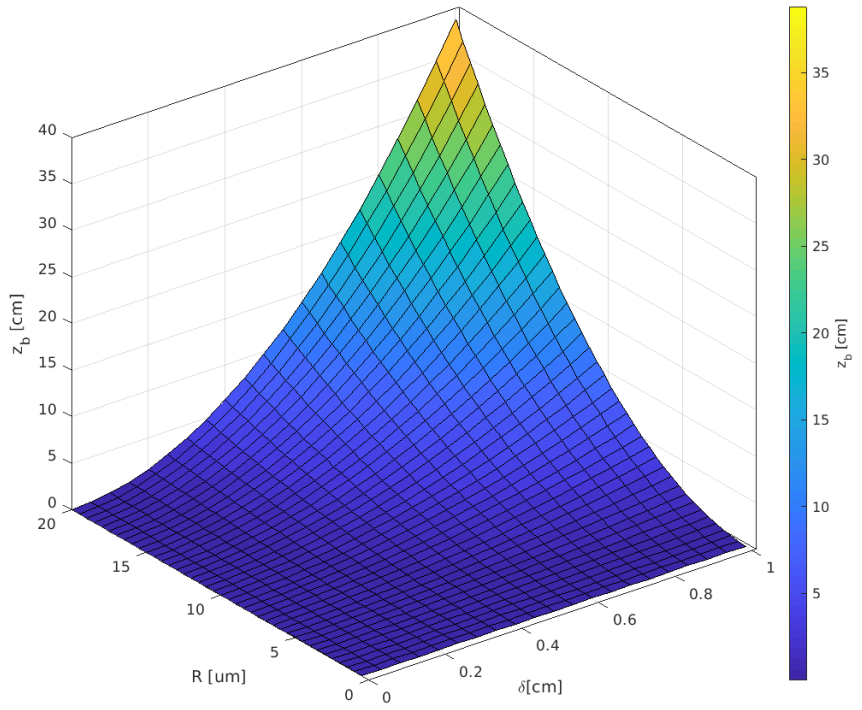

Rysunek 1: Equillibrium position z_b versus vortex core size δ and particle radius R. Plot variables' ranges correspond to cloud-like conditions.

The characteristic time of the motion along the axis is τ_z:

$$\tau_z = \frac{2}{k^{-1} - 1}\tau_p = \frac{2}{\sqrt{1 + \nu\tau_p\delta^{-2}} - 1}\tau_p \tag{9}$$

We assume that particle is small, i.e. crucially smaller then vortex size: $R << \delta$. Then $\tau_p << \gamma^{-1}$ and τ_z is approximately proportional to the inverse of stretching strength:

$$\tau_z \approx 4\nu^{-1}\delta^2 = 8\gamma^{-1}. \tag{10}$$

Figure 2 presents τ_z dependence on δ (on x-axis) and R (color). The approximated dependence on δ (or equivalently - on stretching strength γ) as written in Eq.14 is shown with a blue line. We see that for cloud-like variables' ranges depicted in the Fig. 2 the dependence on particle size is weak and the approximation is justified. In cloud-like conditions τ_z is significantly greater then τ_p.

Of obvious, in turbulence the Burgers vortex is a good approximation for a real field of a long-lasting vortex only locally. Therefore, the motion of particles in a vortex with a finite size and lifetime should be considered. For this reason we discuss and estimate below what we call "exit time" t_{ex}: time at which a particle reaches an arbitrary position Z (or $-Z$) (domain boarder), while its initial position is $z(t = 0) = z_0$ and initial velocity is zero $\dot{z}(t = 0) = 0$.

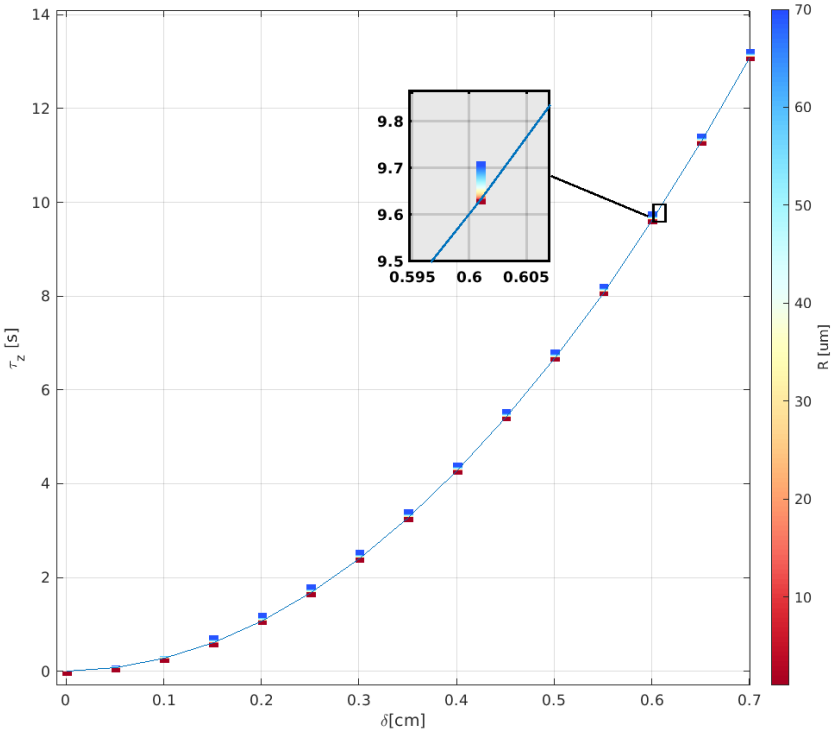

Rysunek 2: Characteristic time of the motion along vortex axis τ_z versus vortex core size δ and particle radius R. Point color indicates dependence on R. Plot variables' ranges correspond to cloud-like conditions. Blue line presents the approximated value as in Eq.14.

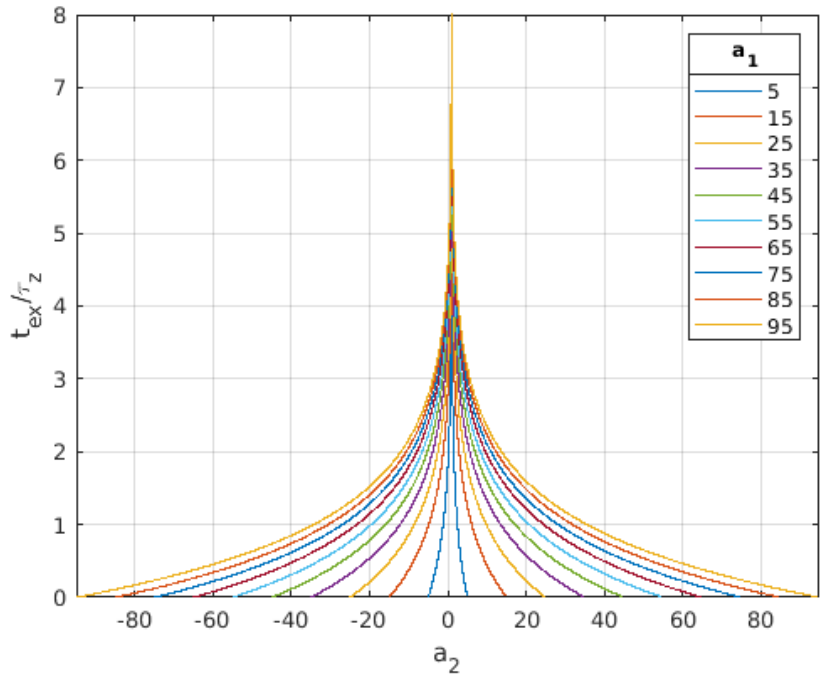

Rysunek 3: Logarithmic factor in t_{ex} vs. ratio of initial position and equillibrium position a_2. Line colors present cases of different ratios of final position (or vortex length) and equillibrium position a_1.

For the purpose of t_{ex} estimation, we first analyse a simplified case of Eq. 8 with $w_0 = 0$:

$$\frac{z(t) - z_b}{z_0 - z_b} = \frac{1}{2}(1-k)\, e^{\frac{-t}{2\tau_p}(k^{-1}+1)} + \frac{1}{2}(1+k)\, e^{\frac{t}{2\tau_p}(k^{-1}-1)} \tag{11}$$

For large times we can approximate Eq.11:

$$\frac{z(t) - z_b}{z_0 - z_b} = \frac{1}{2}(1+k)\, e^{\frac{t}{2\tau_p}(k^{-1}-1)} \tag{12}$$

Exact direction of motion depends on the relative position of z_0 and z_b, so lefthandside of Eq.11 is:

$$L(Z, z_0; z_b) = \frac{Z - \mathrm{sign}(z_0 - z_b) z_b}{|z_0 - z_b|} = \frac{Z/z_b - \mathrm{sign}(z_0 - z_b)}{|z_0/z_b - 1|} = \frac{\overbrace{Z/z_b}^{a_1} - \mathrm{sign}(z_0/z_b - 1)}{|\underbrace{z_0/z_b}_{a_2} - 1|} \tag{13}$$

Then the approximated exit time:

$$\begin{aligned} t_{ex}(a_1, a_2; \tau_z) &\approx \tau_z \log\left(L(a_1, a_2)\right) \\ L(a_1, a_2) &= \tfrac{a_1 - \mathrm{sign}(a_2 - 1)}{|a_2 - 1|} \end{aligned} \tag{14}$$

where we assume $a_1 \in (1, \infty)$, $a_2 \in [-a_1, a_1] \backslash \{1\}$. For $a_2 = 1$ (when $z_0 = z_b$) we have $t_{ex} = \infty$. The logarithmic factor in t_{ex} is depicted in Fig. 3. It depends on vortex length Z and initial position z_0 ratio with respect to z_b.

The mean value of this factor over a_2 equals one for every a_1:

$$\langle \log L(a_1, a_2) \rangle_{a_2} = \frac{1}{2a_1} \int_{-a_1}^{a_1} \log L(a_1, a_2) da_2 = 1 \tag{15}$$

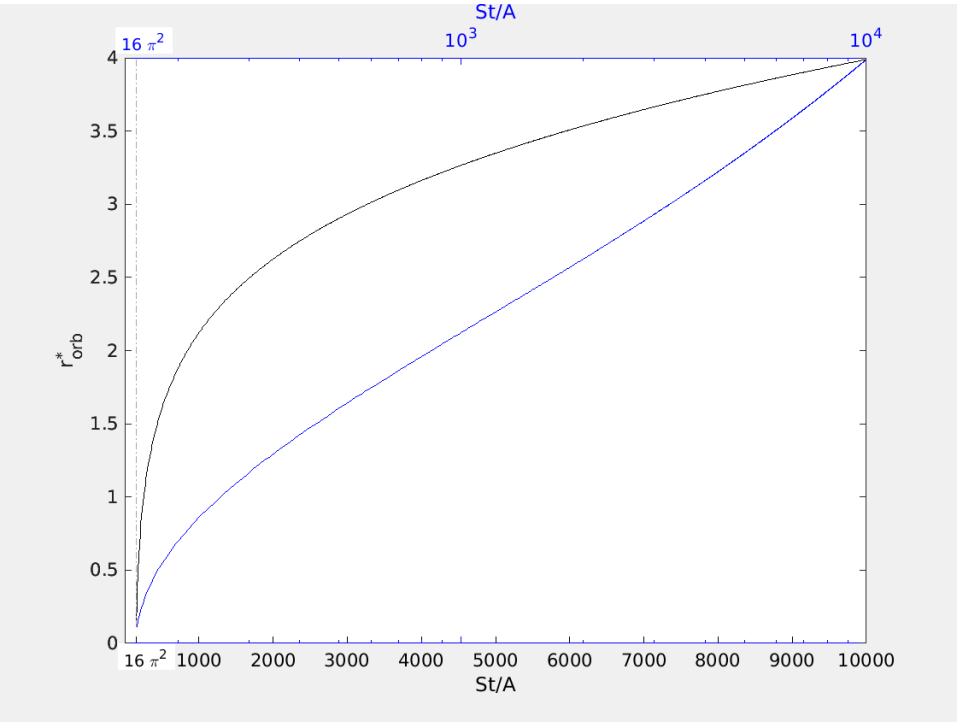

Rysunek 4: Particle stable orbit radius r^*_{orb} dependence on parameter St/A.

Motion in the plane perpendicular to vortex axis

The solutions of Eq.4 have several different attractors in 2D space. It is helpful to distinguish two cases: with gravity and without gravity (valid as well when gravity is parallel to the vortex axis).

Without gravity (vertical vortex)

Since $Sv = 0$ in this case the nondimensional equations of motion are:

$$\begin{cases} \ddot{r^*} - r^* \dot{\varphi^*}^2 = -St^{-1} \left(A r^* + \dot{r^*}\right) \\ 2\dot{r^*}\dot{\varphi^*} + r^* \ddot{\varphi^*} = St^{-1} \left(\frac{1}{2\pi r^*}(1 - e^{-\frac{r^{*2}}{2}}) - r^* \dot{\varphi^*}\right) \end{cases} . \tag{16}$$

and the system is axially symmetric. This set of equations depends on two parameters only: St/A and St.

For every particle of a given St in a vortex of arbitrary strain A a stable, circular periodic orbit exists if:

$$St < St_{cr}(A) = 16\pi^2 A \tag{17}$$

For $St > St_{cr}$, there exists a stable equilibrium point positioned on the vortex axis . Solving periodic orbit set of equations lead to two results. Fristly, radius of the periodic orbit r^*_{orb} satisfies the equation:

$$\left[1 - \exp\left(-r^{*2}/2\right)\right] / 2\pi r^{*2} = \sqrt{A/St}. \tag{18}$$

Equation 18 can be solved numerically. The resulting r^*_{orb} estimation are presented in Fig. 4 for some arbitrary parameter ranges.

This plot suggest that at least for some intermediate St/A values the r^*_{orb} dependence can be close to logarithmic. Secondly every paricle moving on periodic orbit has the same angular velocity (nondimensional): $\omega^*_{orb} = \sqrt{A/St}$, or in other words, particle rotation time

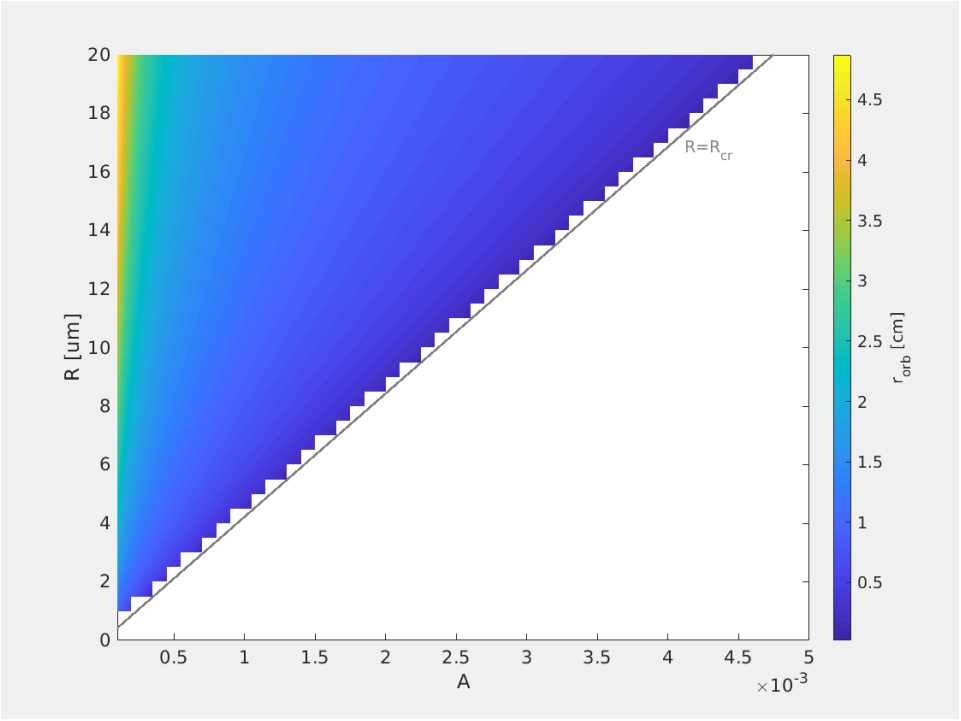

Rysunek 5: Particle stable orbit radius r_{orb} dependence on particle radius R and vortex strain parameter A for cloud-like parameter ranges and vortex core size $\delta = 0.5$ cm. Black line represents stable orbit existence condition.

$\tau^*_{orb} = \sqrt{St/A}$.
A cloud-like view at the periodic orbit issue is considered below. Periodic orbit existence condition 17 is reformulated:

$$R > R_{cr} = 12\pi\sqrt{\rho_a/2\rho_p}\ A\delta \tag{19}$$

The r_{orb} (note: dimensional) calculation results presented in Fig.4 are now shown in the Fig. 5, where vortex core size is chosen arbitrarily: $\delta = 0.5$ cm. We can see that to some extent orbit radius is of vortex core radius order.

It is worth to notice that the dimensional angular velocity ω_{orb} is independent of A. It is in fact inversly proportional to particle radius R and vortex core size δ:

$$\omega_{orb} = \sqrt{A/St}\tau_f^{-1} = \delta^{-1}\sqrt{\nu\tau_p^{-1}} = \sqrt{\gamma(2\tau_p)^{-1}} = 3\nu\sqrt{\rho_a/2\rho_p}(R\delta)^{-1} \sim (R\delta)^{-1}. \tag{20}$$

Fig. 6 presents cloud-like values of angular velocity ω_{orb}. It is itself independent of A, but it is the periodic orbit existence condition that depends on A. The existence condition is presented in Fig.6 by $R = R_{cr}(A)$ plots. For a given A periodic orbits exist in $R > R_{cr}(A)$ area.

Particle rotation time being an inverse of angular velocity is proportional to vortex core radius and particle radius:

$$\tau_{orb} = \sqrt{2\tau_p/\gamma} \sim R\delta. \tag{21}$$

The previously established assumption of small particles i.e. $\tau_p << \gamma^{-1}$ leads to the conclusion that $\tau_{orb} << \gamma^{-1}$ as well. Eventually, bearing in mind relation 10, it is $\tau_{orb} << \tau_z$. As long as the logarithmic

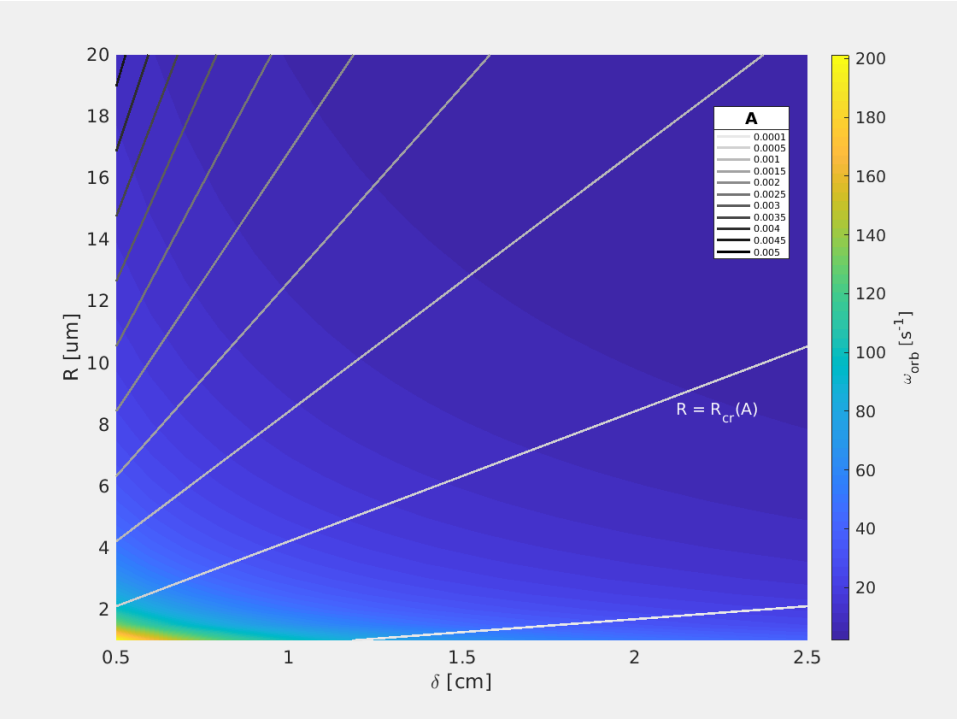

Rysunek 6: Particle stable orbit angular velocity ω_{orb} dependence on particle radius R and vortex core radius δ for cloud-like parameter ranges.

part in Eq.14 is not significantly smaller than 1, then $\tau_{orb} << \tau_{ex}$. It means that particle under such condition is able to swirl around the vortex axis before being expelled by motion along vortex axis.
We define docking time t^*_{doc} as time at which particle can reach its destined radial position. This 'docking process' occurs twofold, because every particle is either attracted by its stable point at $r^* = 0$ or by its stable orbit r^*_{orb}. Consequently the docking time t^*_{doc} is time at which particle positioned at:

- $r^*(0) = 0$ can reach its periodic orbit r^*_{orb}
- positioned at $r^*(0) = r_s$ can reach $r^* = 0$.

According to these definitions numerical analysis of t_{doc} for arbitrary parameter ranges was conducted. However due to the facts that $r^* = 0$ the particle approach its destined radial position asymptotically, the docking time was calculated numerically between positions:

- $r^*(0) = \epsilon$ and $r^*(t^*_{doc}) = r^*_{orb} - \epsilon$,
- $r^*(0) = r_s$ and $r^*(t^*_{doc}) = \epsilon$.

Figure 7 and 8 present the results of t^*_{doc} numerical calculation, with respect to St and A in 3D and 2D plots respectively. Blank spaces in the figures represent sets of parameters for which calculation was numerically expensive and hence the result was not included. Vertical axis in 7 and colorscale in both figures are logarithmic. Black line in Fig. 8 respresents the $St = St_{cr}(A)$.

From the Fig. 7 and 8 it is clear that the most striking results are retrived near $St = St_{cr}(A)$.

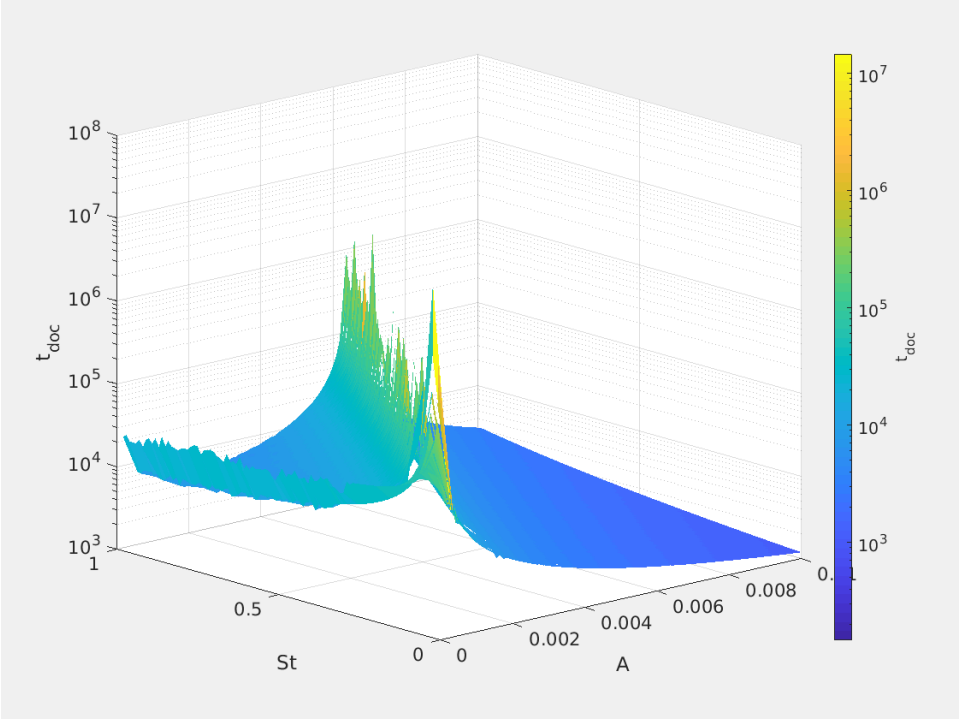

Rysunek 7: Docking time calculated numerically with respect to St and A for arbitrary variable ranges with $\epsilon = 10^{-5}$. Blank spaces represent lack of data, numerically too expensive.

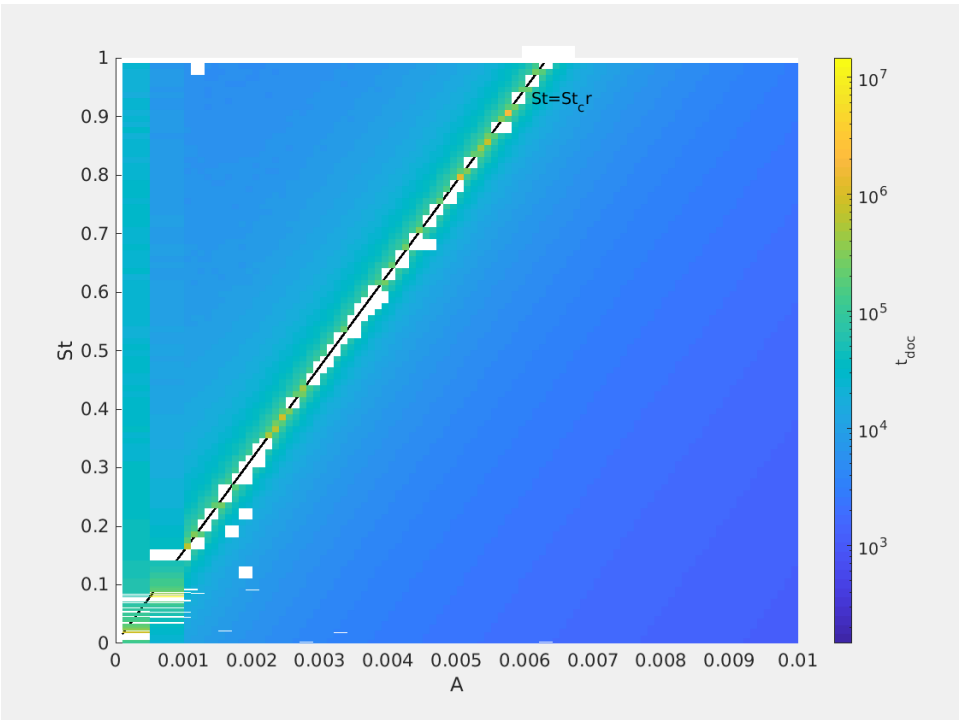

Rysunek 8: The same as in Fig. 7, projection. Black line $St = St_{cr}(A)$ shows the stability boarder: particles to the left are attracted by periodic orbits, particles to the right by stable points on vortex axis.

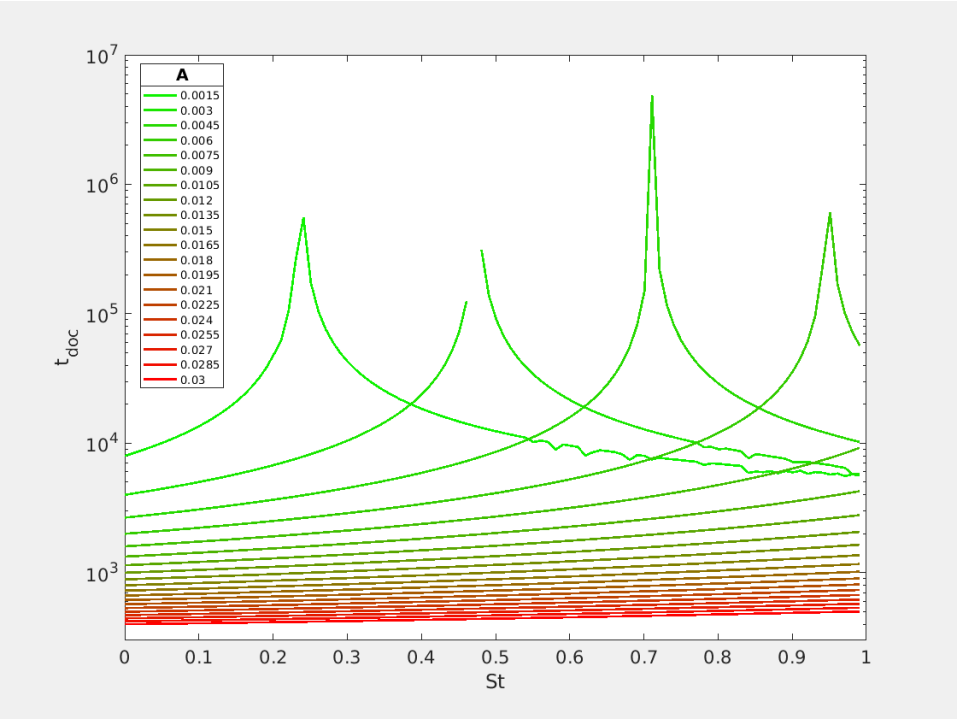

Rysunek 9: Docking time calculated numerically with respect to St for a few chosen A values, $\epsilon = 10^{-5}$.

Tu pare wniosków i opis co widac na rysunkach:
Rys.6,7

- zmiany wartości są ciagle, co moze swiadczyc o dobrej definicji t_doc?
- wyrazne szalone (log!) maksimum wokol $St = St_{cr}$, poniewaz sila dzialajaa na czastke jest malutka
- Dla $St < St_cr$ glownym parametrem wydaje sie byc St/A razy cos tam, bo linie sa prawie rownolegle dla malych A wzrost czasu prawie wylacznie ze zmniejszajacym sie A - orbity sa tak daleko?

Rys.8,9,10 - czy widac jakakolwiek zaleznosci analityczna dla St albo A

Since ϵ in theory is infinitesimally small but the numerical calculation demands finite value, the sensitivity analysis was conducted below for $\epsilon = 10^{-n}$, $n = 1, 2, 3, 4, 5$.

With gravity (inclined vortex)

Nonparallel alignment of the gravity vector and vortex axis ($\theta \neq 0$) destroys the axial symmetry of the system and introduces the presence of other attractors, such as limit cycles and equilibrium points outside the axis.

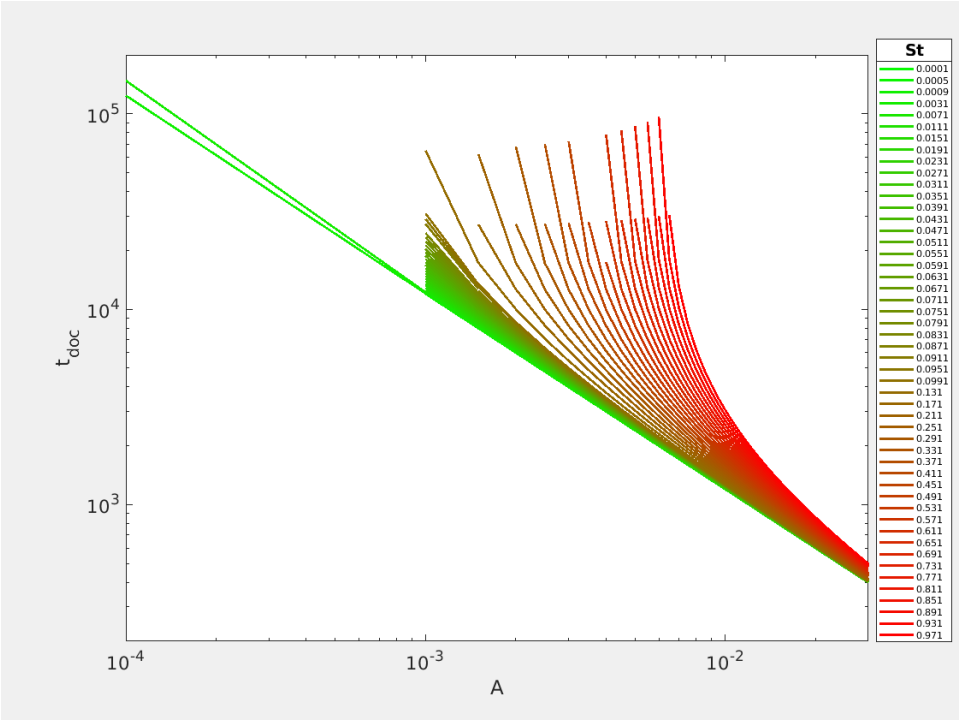

Rysunek 10: Docking time calculated numerically with respect to A for a few chosen St values, for $A > St/16pi^2$, $\epsilon = 10^{-5}$.

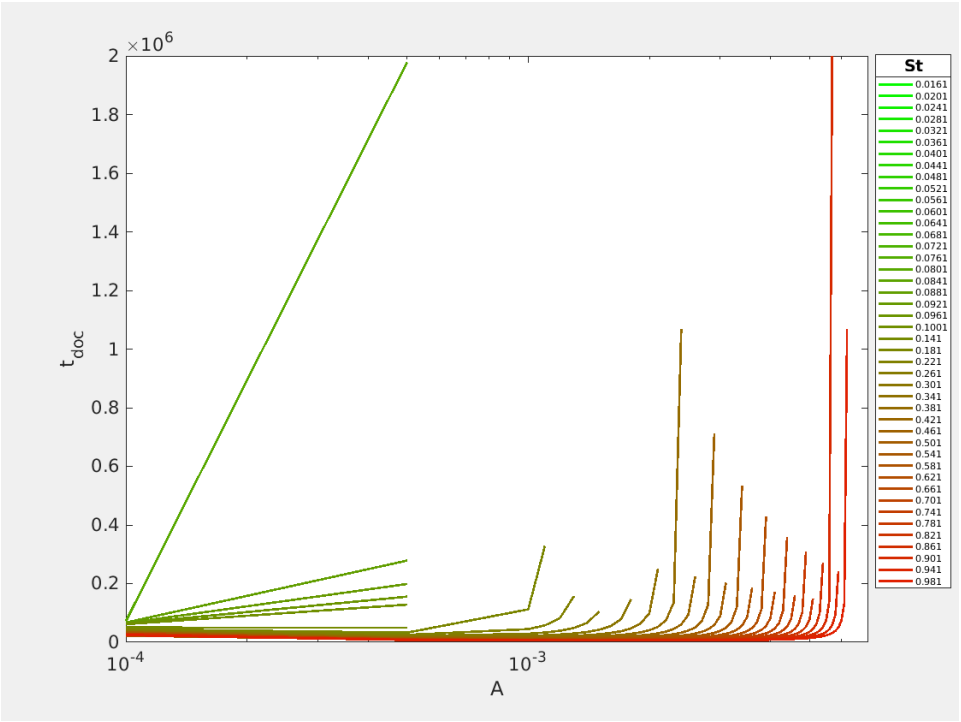

Rysunek 11: Docking time calculated numerically with respect to A for a few chosen St values, for $A < St/16pi^2$, $eps = 10^{-5}$.

Tablica 1: Existence of equilibrium points with respect to A and S_ν parameters. A_{cr}, r^*_s, r^*_{min}, $S_{\nu\ min}$, $S_{\nu\ max}$ defined in the text body.

A A_{cr}	S_ν - arbitrary	1 eq. point
$A < A_{cr}$	$< S_{\nu\ min}$	1 eq. point at $r^* < r_s$
	$[S_{\nu\ min}, S_{\nu\ max}]$	2 or 3 eq. points
	$> S_{\nu\ max}$	1 eq. point at $r^* > r_{min}$

Tablica 2: Burgers vortex non-dimensional numbers

A_{cr}	0.02176
r^*_i	2.1866
r^*_s	1.585201
A_t	0.01917

For a nonzero θ, every particle always has equilibrium points in 2D space. Positions of these points are determined by S_ν and A. They can be obtained by solving the equation for the radial component r^*:

$$r^* A \sqrt{1 + \left(\frac{1 - \exp\left(\frac{-r^{*2}}{2}\right)}{2\pi A r^{*2}} \right)^2} = S_\nu. \tag{22}$$

Now, let $f_A(r^*)$ be the left hand side of Eq. 22. A plot of this function for a given A is called an equilibrium curve (see Fig.2 in **Marcu_95**). Detailed analysis of equilibrium curve dependence on parameters is performed below and leads to the conclusions summarised in Table 1.

It is easy to find that $f_A(0) = 0$ and $\lim_{r^* \to \infty} f_A(r^*) = \infty$. Moreover, there exists a critical value A_{cr} for which bifurcation from one unique solution (for $A \quad A_{cr}$) to maximally three solutions (for $A < A_{cr}$) occurs. A_{cr} corresponds to the equilibrium curve that has a horizontal slope at the inflection point. A_{cr} value was estimated numerically (see the Table 2).

For $A \quad A_{cr}$ the equilibrium curve is a monotonically increasing function of r^* so there exists exactly one solution for every S_ν value. For $A < A_{cr}$ the equilibrium curve always has one maximum at r^*_{max} and one minimum at r^*_{min}. The inflection point at $A = A_{cr}$ on the equilibrium curve lies at r^*_i (see the Table 2). It restricts values of r^*_{max} from above and values of r^*_{min} from below.
Consequently, for $S_\nu < f_A(r^*_{min})$ and for $S_\nu > f_A(r^*_{max})$, there is only one solution. For $S_{\nu\ min} = f_A(r^*_{min})$ and for $S_{\nu\ max} = f_A(r^*_{max})$, there are two solutions. For $f_A(r^*_{min}) < S_\nu < f_A(r^*_{max})$, there are three solutions.
Not only is the existence of the solutions important but their stability as well. Let r_0 denote an arbitrary solution of Eq. 22. The exact form of the stability condition of the solution r^*_0 is governed by the function $\phi(r^*_0)$ (as defined in **Marcu_95**). The condition can take two different forms depending on the sign of this function

$$\phi(r^*_0) = \frac{1}{(2\pi)^2} \left[\frac{1 - \exp(-r^{*2}_0/2)}{r^{*2}_0} \right] \left[\frac{1 - \exp(-r^{*2}_0/2)}{r^{*2}_0} - \exp(-r^{*2}_0/2) \right].$$

Tablica 3: Stability conditions of particle equilibrium points present in the Burgers vortex with respect to vortex strain parameter A and dimensionless distance from the vortex axis r^*. A_t, $\varphi(r^*)$, r_s^*, r_{min}^* and r_{max}^* defined in the text body.

	r_s^*	(r_s^*, r_{max}^*)	$[r_{max}^*, r_{min}^*)$	r_{min}^*
$A < A_t$	unstable for $St > A/\lvert\phi(r_0^*)\rvert$	stable	partly unstable	stable
$A \ A_t$		stable		

(23)

The function has only one zero at r_s^* (see Table 2). For small radii ($r_0^* < r_s^*$), the equilibrium is stable if:

$$\frac{St}{A} \quad \frac{1}{|\phi(r_0^*)|}. \tag{24}$$

For greater radii ($r_0^* > r_s^*$), the condition for stability depends explicitly only on A:

$$A \quad \sqrt{\phi(r_0^*)}. \tag{25}$$

The equilibrium point satisfying the first type of the condition was shown to be a focus, the second type to be a node.
Analysis of the equilibrium point stability conditions by **Marcu_95** is expanded here with emphasis on the dependence on strain parameter A. The results are described in detail below and summarised in Table 3.

Generally, stability conditions are different for A ranges separated by $A_t = \max_{r_0^*}\left(\sqrt{\varphi(r_0^*)}\right)$ (approximate value obtained numerically in Table 2). $A > A_t$ always satisfies then the condition expressed by 25. The term "partly unstable"in the table refers to the following: In the range of $r_{max}^* \quad r_0^* < r_{min}^*$, for a given A, only a small fraction of the total range (near points r_{max}^* and r_{min}^*) is stable. This range grows with increasing A. Numerical experiments show, however, that their domain of attraction in the presence of other stable points (at least one exists always) is relatively small.

The combination of multiple existence conditions with stability conditions creates a variety of single particle motion scenarios. Some of them are shown in Fig.4 in **Marcu_95**. These scenarios are used in the next section to carry out a search for vortex model parameter values that produce a void. Fig. **??** here illustrates one of these scenarios in which there are three equilibrium points: I - unstable point near the axis, II - unstable middle distance point, III - stable point far from the axis. A particle, depending on initial position and velocity, rotates around point I or is weakly attracted by unstable point II or is strongly attracted by stable point III.